Optimization of offshore direct drive wind turbine generators with consideration of permanent magnet grade and temperature

Nurul Azim Bhuiyan and Alasdair McDonald

***Abstract*— In this paper, the main objective is to optimize permanent magnet synchronous generators for offshore direct drive wind turbine, examining the best choice of magnet grades, BH_{max} and working temperature. A surface-mounted Nd-Fe-B generator is designed electromagnetically and structurally and optimized for different rated powers of 6, 8 and 10 MW. The results show that the cost of energy decreases as the wind turbine's rated power increases. Further optimizations were carried out using different neodymium magnet grades and it was found that the higher magnet grades produce a lower cost of energy. In addition, steps were taken to estimate the effect of magnet temperature. A detailed thermal model is used to calculate the cooling airflow requirements to bring the magnet operating temperature from 120°C to 80°C. Allowing the use of cheaper temperature grades of magnets, the additional cooling reduces winding losses and improves the effective BH_{max} of the magnets.**

***Index Terms*—Cooling system, cost of energy, magnet grade, optimization, permanent magnet generator, thermal model, wind turbine.**

I. Introduction

The rated power capacity of offshore wind turbines is increasing rapidly. In recent years, the turbine power generation abilities are increasing from the 6 MW to 10 MW and beyond. A large number of wind turbine designs in offshore are now direct-drive permanent magnet (PM) synchronous generators. It is mainly attractive to use because of lower maintenance cost, high efficiency and longer life as gearboxes are less reliable and incur mechanical losses [1], [2]. However, the bigger size, the large quantities of rare earth permanent magnet materials, mass and the massive generator structures are the main challenges for designers of direct-drive permanent magnet generators [3].

The torque (and hence the power production at a given speed) is directly proportional to the air-gap shear stress and making machines more compact requires improvements in shear stress. This shear stress is proportional to the product of the magnetic loading (related to the air-gap flux density) and the electrical loading (related to the current density) and efforts to maximize this shear stress can generally be categorized according to which of these loadings are improved. The improvements in maximum energy product, BH_{max} of modern PM materials, designs of magnetic circuits and the choice of iron materials have steadily helped improve the magnetic loading (or the effective cost of this magnetic loading). The careful selection of winding arrangements and improvements in manufacturing techniques have helped to improve both winding factors and fill factors and hence electrical loading. Improvements in cooling help improve both magnetic and electrical loading. The *BH* characteristics of PM materials are temperature dependent, so cooling them improves the effective remanent flux density. The heat circulation from the stator windings and iron cores to the rotor where permanent magnets are mounted should make minimum as the magnet materials are temperature sensitive [4]. In most direct drive generators, I^2R losses dominate. As the electrical resistivity of most conductors is generally temperature dependent, cooling also helps machines operate at higher electrical loading or with smaller losses.

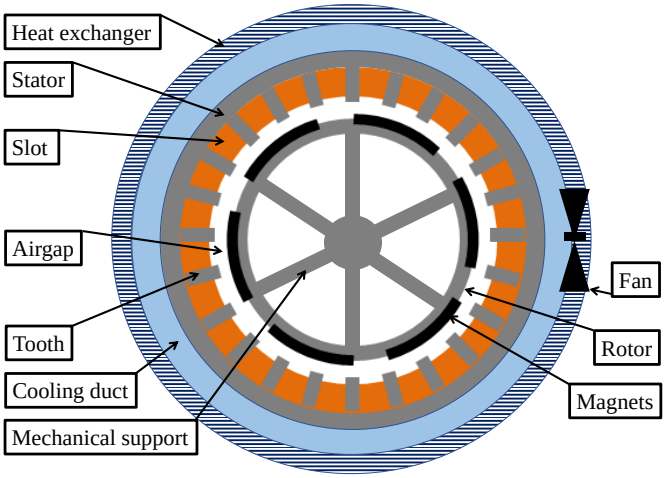

Fig. 1. A simple direct-drive generator for wind turbine with active materials, mechanical support and cooling system.

Different cooling methods can be used. Grauers shows a method where the outer surface of the generator stator core is cooled by cooling channels using forced air [5]. Alexandrova *et al.* manage the losses of the stator winding due to joule heating by internal direct liquid cooling [6]. Others have looked at different cooling methods and coolants [4], [7], [8]. During an optimization processes, authors often assume that the winding and magnet temperatures are constant, e.g. [9]. In this study a comprehensive thermal model is used to include this aspect during optimization.

Different authors have approached different optimization methods with different objective functions to minimize the generator cost of active materials, cost of structural materials, losses, masses and maximize the efficiency and annual energy productions [5], [10-13]. A hybrid algorithm combining

N. A. Bhuiyan is with ASTUTE, College of Engineering, Swansea University, Swansea SA1 8EN and A. McDonald is with the Institute of Energy and Environment, Department of Electronic and Electrical Engineering, University of Strathclyde, Glasgow G1 1XW, United Kingdom. (e-mail: n.a.bhuiyan@swansea.ac.uk; alasdair.mcdonald@strath.ac.uk).

Genetic Algorithms (GA) with Pattern Search (PS) is used in [9]. In this method, after a few generations the GA produces an intermediate global solution which is then taken as primary input by the PS to run a local search. The result after the local search from this PS is taken as the global optimum result.

The main emphasis of this paper is to optimize large, low speed direct drive generators using different rated power (6, 8 and 10 MW) for offshore wind turbine operation, exploring a number of issues that attract a typical wind turbine generator designer: the effect of different neodymium magnet grades (N35 to N52) in the generator rotor, estimate the effect of temperature due to losses by accumulation of a generator thermal model and cooling down magnet temperature (from 120°C to 80°C) using the cooling system and controlling the cooling air flow for variable losses.

In this paper, a 6 MW surface-mounted Nd-Fe-B (SM Nd-Fe-B) generator is designed by following the work of McDonald and Bhuiyan [9], using flexible boundary limit for optimization to allow the maximum air-gap diameter. This 6 MW generator is then upgraded to 8 and 10 MW and compared with 6 MW SM Nd-Fe-B generator after optimization for offshore wind turbine application. These are analytically designed and optimized in MATLAB and verified using finite element software. Two different objective functions are used for optimization to compare the best performance machine. Further optimizations were carried out for a 6 MW Nd-Fe-B generator using different neodymium magnet grades (N35 to N52) and operating temperature ("H" grade where maximum operating temperature 120°C and "Regular" grade where maximum operating temperature 80°C). In addition, steps were taken to estimate the effect of magnet temperature. A detailed thermal model is used to calculate the cooling airflow requirements to bring the magnet operating temperature from 120°C to 80°C. A number of fans and heat exchangers are used for the cooling system. The process of controlling cooling air flow for variable losses also shown after that.

II. Methodology

The turbine characteristics for this study is defined in this section. The generator model that includes electromagnetic and structural model comes after that. Next, the structural model of the tower, substructure and foundation costs of the wind turbine are described. The investigations include the effect of using different magnet grades in generator rotor and a thermal model to estimate the effect of temperature due to losses and cooling costs are defined after that. Subsequent to that, the process of optimization is described.

A. Wind Turbine Characteristics

In this study, a generic variable speed, 3-bladed, pitch regulated wind turbine is modeled for an offshore application. The major ratings and assumptions for three different rated powers are given in Table I. It is presumed that the turbine rotor speed varies proportionally with the wind speed below the rated speed. The rotor speed becomes constant when it reaches to rated wind speed and power and blades are pitched. Table I shows the wind speed characteristics to define the probability of the wind speed.

B. Generator Model

The SM Nd-Fe-B generator is modeled analytically in the steady state using MATLAB. Lumped parameter magnetic circuit models are used to calculate flux per pole.

The N40H magnet is chosen as the baseline magnet in this study and its properties are given in Table IV. Fig. 2 shows the generalized, geometrically linearized sections of generator model for one pole pair. This magnetic circuit is also modeled in FEMM to verify the results from analytical model [16]. The calculation of flux density and induced emf using the magnetic circuits can be found as shown in [17]. Table II shows some key dependent variables verified using a 2D finite element software (FEMM) for the baseline generator design.

The electrical equivalent circuit modeling, losses, output power, masses of different materials and costs calculation are the same as the method in [9] and [17]. The assumed costs in Table III for different materials are taken from [9] and [11]. Generator structural modeling given in [9] is used in this study where the deflections of structure are limited in three directions radially, tangentially and axially in optimization process to minimize the structural mass.

TABLE I
THE WIND TURBINE SPECIFICATIONS AND SITE WIND RESOURCES [9]

Rated wind speed (m/s)			11
Cut in wind speed (m/s)			3
Cut out wind speed (m/s)			25
Optimal tip speed ratio			8.3
Coefficient of performance at optimal tip speed ratio			0.48
Wind turbine availability (%)			94
Site wind speed shape parameter			2.3
Site wind speed scale parameter (m/s)			10.8
Mean wind speed (m/s)			9.6
Turbine characteristics for different power ratings			
Rated grid power (MW)	6	8	10
Rotor diameter (m)	145	166	185
Rated rotational speed (rpm)	12	10.5	9.4
Hub height (m)	90	100	110
Fixed charge rate (FCR)	0.116	0.116	0.116
Wind firm turbine capital cost (exc. Generator, tower and foundation) (k€) [14]	16309	20564	24948
Operation and maintenance cost (k€) [15]	628	816	1005

.

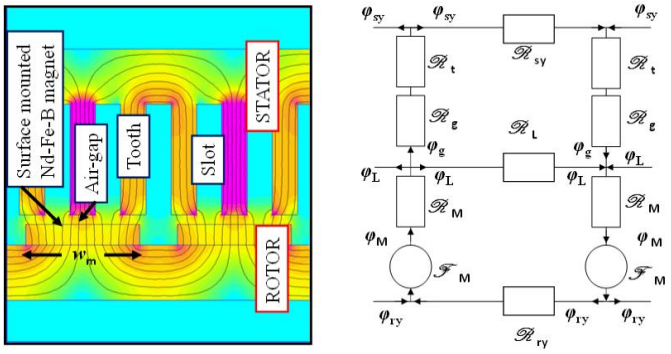

Fig. 2. (a) Magnetostatic finite element analysis of surface-mounted Nd-Fe-B generator, (b) Magnetic circuit. ■0T→■1.5T. Software is FEMM [16]

TABLE II
ANALYTICAL RESULTS VS FEMM ANALYSIS RESULTS

Variables	Analytical	FEMM
Fundamental air-gap flux density, B_g (T)	1.00	0.99
Direct axis inductance, L_d (mH)	18.4	18.2
Quadrature axis inductance, L_q(mH)	18.4	18.2

TABLE III
GENERATOR MATERIALS AND COST MODELING [9], [11]

Generator Material Characteristics	
Slot filling factor	0.6
Resistivity of copper at 120ºC (μΩ·m)	0.024
Temperature coefficient of resistivity (K^{-1})	0.00393
Eddy-current losses in laminations at 1.5 T, 50 Hz (W/kg)	0.5
Hysteresis losses in laminations at 1.5 T, 50 Hz (W/kg)	2
Cost Modeling	
Lamination cost (€/kg)	3
Copper cost (€/kg)	15
Permanent magnet cost (N40H magnet) (€/kg)	60
Rotor iron cost (€/kg)	2
Structural steel cost (€/kg)	2
Price of kWh energy (€/kWh)	0.19

C. Magnet Grades

When choosing the type of Nd-Fe-B magnet, a generator designer can pick from a number of magnet grades. These grades are often expressed as N*XY* where 'N' indicates that this is an Nd-Fe-B magnet, *X* is the maximum energy product (BH_{max}) in MGOe and *Y* indicates the maximum working temperature. Although the actual *BH* of a magnet depends on the magnetic circuit design in which it is placed, BH_{max} is a good figure of merit and a higher number indicates a stronger magnet.

The production of rare earth permanent magnets is based on the combination of intermetallic compounds of rare earth elements and the transition metals Fe or Co. The development in the last few decades has led to significant improvements in energy product BH_{max} and higher Curie temperatures (the temperature at which the magnet will become completely demagnetized) [19-20].

Gutfleisch [19] shows different manufacturing routes of magnets for high BH_{max} and high operating temperatures. Based on the proportion of intermetallic compounds of rare earths, transition metals, other impurities, structure, heat treatment and processing route, BH_{max} and the maximum operating temperature and the cost of a magnet will be different. Commercial magnetic characteristics are advertised with tolerance; where an operative range of the maximum energy product are given.

TABLE IV
MAGNETIC PROPERTIES FOR DIFFERENT MAGNET GRADES [18]

Magnet grade	Remanent flux density (T)		
	Regular	"H" grade	
Operating Temperature	80˚C	80˚C	120˚C
N35	1.12	1.12	1.06
N38	1.17	1.17	1.11
N40	1.20	1.20	1.13
N42	1.21	1.21	1.15
N45	1.25	1.25	1.19
N48	1.30	1.30	1.23
N50	1.32	1.32	1.25
N52	1.34	1.34	1.27

A number of different Neodymium magnet grades (N35 to N52) are used in this study for a 6 MW SM Nd-Fe-B generator. The baseline neodymium magnet grade in this study is N40H. The optimization process is repeated for other magnet grades and the optimal designers are compared. Table IV shows the magnetic properties, the maximum operating temperature of different Neodymium magnet grades and their actual operating temperatures. The current specific per unit cost of different magnet grades are collected from [21] and [22], are shown in Fig. 3. The cost of different magnet grades, C(*X*) can be found from the baseline magnet cost C(40H) given in Table III, multiplied with unit price, *U* given in Fig. 2.

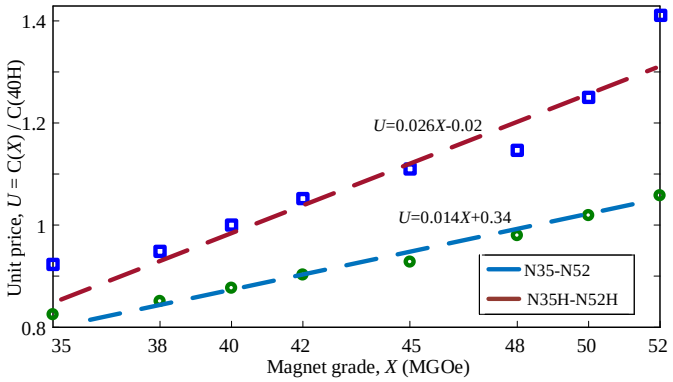

Fig. 3. Fitted trend lines of the per unit specific cost of Nd-Fe-B magnet grades (relative to N40H). *X* represents the maximum energy product and the graph shows 'regular' and high temperature magnets. [21-22]

D. Temperature Effect and Cooling

It is important to understand the effect of operating temperature on Nd-Fe-B magnets. Typically, Nd-Fe-B magnets operate best at lower temperatures, i.e. their B_r and H_c are larger. Regular Nd-Fe-B magnets can work safely up to 80ºC temperature but after this point, they begin to irreversibly lose their magnetism. On the other hand, grades with an "H" rating can operate in temperatures up to 120˚C.

This study estimates the temperature effect due to power losses, the additional cost and energy consumption incurred to cool down the magnet temperature by forced air flow using fan and heat exchanger. Different "H" grade Nd-Fe-B magnets (N35H –N52H) with operating temperature of 120˚C are used in the rotor of 6 MW SM Nd-Fe-B generator to estimate the temperature rise due to losses. After that a cooling system is introduced to cool down the magnet temperature 120˚C to 80˚C. Subsequent to that, different regular grade magnets (N35-N52) with maximum operating temperature of 80˚C are used instead of "H" grade magnet to compare the effect of temperature and cost of energy. The process of controlling the cooling air flow for variable losses comes after that.

1) Temperature Effect on Resistance and B_r

In the case of additional cooling, the winding temperature will be decreased. The resistivity, ρ_r dependency on temperature is,

$$\rho_r(T) = \rho_0(1 + \alpha\Delta T) \quad (1)$$

where ρ_0 is the resistivity at ambient temperature (20˚C) and α is the temperature coefficient of copper. This varying resistivity affects the winding resistance. The copper losses of the generator vary due to temperature effect on resistance.

The magnet's remanence (B_r) and coercivity vary with temperature as given in [18]. Indeed, changing the temperature of a N40H magnet from 120°C to 80°C will increase its effective BH_{max} by more than 12%. This in turn affects the magnetomotive force, hence the flux density and power production will vary with temperature.

2) Thermal Model

A detailed thermal model based on the work of Grauers [5] is used in this study. A lumped-parameter thermal network model is used to define the 6 MW SM Nd-Fe-B generator. A simplified thermal model for the complete generator given in Fig. 3. The simplified model reduces thermal resistance from the detailed model using symmetry by connecting Q parallel models for a stator slot pitch, coil, 2 p parallel models for a rotor pole and the model for the internal air and the two end shields (where Q is the number of slots and p is the pole pair). The reason behind the simplification is to assess only essential nodes to calculate the winding and magnet temperatures, where the simplified thermal resistance are the replacement of the series and parallel connected thermal resistances. This simplified model consists twelve nodes and eighteen thermal resistances as shown in Fig. 4.

The temperature differences in the circumferential direction of the generator are neglected, i.e. losses are uniformly distributed from one tooth to the next, one slot to the next and one pole to the next. The two end windings of a coil are simplified as one because of symmetrical generator cooling in the axial direction.

The losses are assumed to be dominated by the copper losses come from stator winding, iron losses come from the stator teeth and yoke, eddy current losses come from the magnets and supplementary, stray losses (at no load, 20% of the core losses). It is assumed that, Friction and windage losses do not affect the temperature rise of the winding or magnets, hence they are neglected. The copper losses are divided into losses in the end windings and in the top and bottom coil sides in the slots. The losses in the magnets are assumed to be spread equally, while supplementary losses are expected to be in the tooth tip.

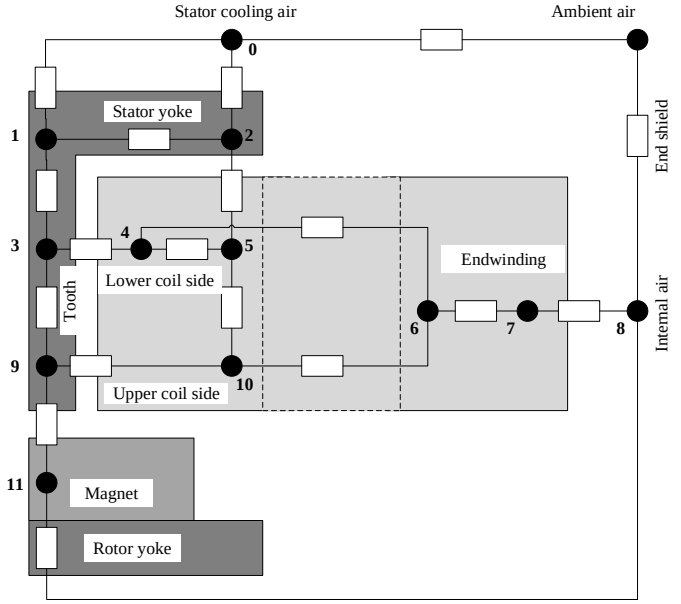

Fig. 4. The simplified thermal model based on one slot pitch, one rotor pole, one coil, internal air and end shield

Cooling Air is passed through circumferential cooling channels to cool down the generator outer surface of the stator core. An equivalent thermal resistance is added in the model to represent the temperature increase in the cooling air. A matrix equation is used to formulate the temperature rise problem. The temperature difference, ΔT between the nodes across a given thermal resistance, R_{th} which results from power losses at specific node, P_{loss} (losses in different nodes and thermal resistance across the nodes can be calculated as Grauers [5]) can be given as,

$$\Delta T = P_{\text{loss}} R_{\text{th}} \tag{2}$$

The temperature rises vector is calculated by multiplying the loss vector by the inverse of the thermal conductance matrix. The analytical results of thermal model are verified using 2D FEMM heat flow analysis [16]. Table V shows some nodes temperature verified using finite element software for the baseline generator design.

The 3D components of the thermal model such as end shield and cooling channel are represented using equivalent conductivity. For the end shield, the equivalent conductivity can be calculated as,

$$\lambda_{\text{end}} = \frac{h_{\text{FEMM}}}{2 l_{\text{s}} R_{\text{th,end}} \pi r_{\text{s,out}}} \tag{3}$$

where h_{FEMM} is the chosen height in FEMM for end shield, $R_{\text{th,end}}$ is the thermal resistance of the end shield and $r_{\text{s,out}}$ is the outer radius of the stator.

TABLE V
ANALYTICAL RESULTS VS FEMM HEAT FLOW ANALYSIS RESULTS

Nodes	Analytical (°C)	FEMM (°C)
Yoke above a tooth	134.2	133.8
Bottom coil side in a slot	145.2	144.9
Top coil side in a slot	150.1	149.7
End winding	153.8	153.6
Magnet	80.1	79.8

3) Air Flow

The volumetric cooling air flow is varied to determine the required air flow to cool down the magnet temperature from 120°C to 80°C. This varying cooling air flow, q_{vc} varies the temperature rise of the cooling duct, which can be represented as equivalent thermal resistance, $R_{\text{th,cool}}$ given in [5],

$$R_{\text{th,cool}} = \frac{1}{q_{\text{vc}} \rho_{\text{c}} k_{\text{thc}}} \tag{4}$$

where ρ_{c} is the density and k_{thc} is the specific heat capacity of the cooling air. Fig. 11(c) shows the trend line of required cooling air flow for a 6 MW Nd-Fe-B generator using N40H magnet, cool down to different magnet temperature.

Typically, a wind turbine generator that is forced air-cooled has a closed loop system which transfers heat from the generator to heat exchangers mounted on the nacelle, where the heat is radiated to the outside air which is at ambient temperature. The flow rate in such a closed system is defined by the characteristics of the fan(s) and the characteristic of the loop. A given fan at a given speed and power input will produce a range of flow rates, depending on how much resistance to flow there in the loop. Its operating characteristic is given by a curve, showing that it has low flow rates when it works at higher pressure but higher flow rates when it works at lower pressures. The pressure that it has to work at is effectively determined by the "resistance" of the loop to air flow. The equation associates to pressure drop, P to volumetric cooling air flow and the system resistance to airflow, R_{sys} can be found by using the equation given as [23],

$$P = R_{\text{sys}} {q_{\text{vc}}}^2 \tag{5}$$

The flow path with all changes are presented by system flow resistance can be calculated as [23],

$$R_{\text{sys}} = \frac{k_{\text{f}} \rho_{\text{c}}}{2A^2} \tag{6}$$

where k_{f} is the coefficient of related fluid resistance that depends on the nature of flow (obstruction, expansion, contraction, and so on). The k_{f} factors for all changes in the air flow path from fan to heat exchanger can be calculated from the formulation given as [23] and [24]. A is the flow section area.

4) Cooling Fan and Heat Exchanger

A number of fans are used and their combined pressure-airflow characteristics [25] can be modeled as a quadratic function as shown in Fig. 5. This figure also shows the system flow resistance curve, the heat exchangers' resistance curve [26] and the combination to give the total system resistance curve, also modeled as a quadratic function. The actual air flow (due to combination of fans and heat exchangers) can be found at the point where the fan curve and the system resistance curves crosses. Table VI gives the specification of a single fan at its maximum speed and the cost of fan and heat exchanger.

A number of fans are needed for the required cooling and these can be used in series and parallel combination. For the case of identical fan units in parallel, the volumetric airflow (at a given pressure) of one fan is multiplied by the number of fans in parallel.

TABLE VI
FAN AND HEAT EXCHANGER SPECIFICATION [25], [26]

Maximum fan power (W)	430
Maximum fan current (A)	2
Maximum fan speed (r/min)	1500
Maximum fan pressure (Pa)	250
Maximum fan airflow (m^3/s)	0.53
Cost of single fan (€)	180
Cost of single heat exchanger (€)	673

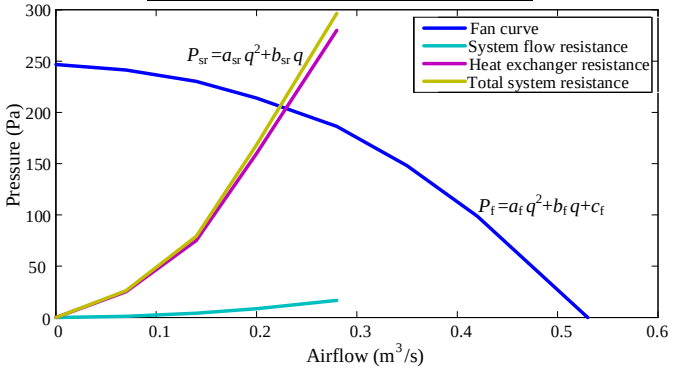

Fig. 5. Fan, heat exchanger and system resistance curve

For the case of series fans, the pressure (at a given airflow) of one fan is multiplied by the number of fans in series. It is important to note that if the fans in combination are not identical, the weaker fan becomes an additional resistance on the system [24]. The combination of series and parallel fan gives a combined characteristic curve which crosses the total system resistance curve and hence the resultant volumetric air flow, q_{vc} at intersecting point can be found as,

$$q_{\text{vc}} = \frac{-\left(\frac{b_{\text{f}}F_{\text{S}}}{F_{\text{P}}} - b_{\text{sr}}\right) - \sqrt{\left(\frac{b_{\text{f}}F_{\text{S}}}{F_{\text{P}}} - b_{\text{sr}}\right)^2 - 4\left(\frac{a_{\text{f}}F_{\text{S}}}{{F_{\text{P}}}^2} - a_{\text{sr}}\right)(c_{\text{f}}F_{\text{S}} - c_{\text{sr}})}}{2\left(\frac{a_{\text{f}}F_{\text{S}}}{{F_{\text{P}}}^2} - a_{\text{sr}}\right)} \tag{7}$$

where a_{f}, b_{f} and c_{f} represents the fan curve coefficients, a_{sr}, b_{sr} and c_{sr} represents the total system resistance curve coefficients, F_{s} is the number of fans in series and F_{p} is the number of fan in parallel. The total cost of fan, C_{fan} used for cooling can be calculated as,

$$C_{\text{fan}} = C_{\text{fmn}} + C_{\text{fen}} \tag{8}$$

where C_{fmn} is the manufacturing cost of the total number fan and C_{fen} is the cost of electricity consumed by those fans, which can be calculated by using data from Table VI. The required heat exchangers are connected in parallel; hence the number of heat exchangers are proportional to the required cooling air flow. The cost of each heat exchanger can be found in Table VI.

5) Air Flow Control at Variable Wind Speed

The variable wind speed before rated wind speed causes variable power losses, hence the required cooling air flow varies, and it is always less than the required cooling air flow at rated wind speed as shown in Fig. 11(b). After installation of fans for maximum required cooling air flow in rated wind speed, the number of series fan is varied by turning on/off to control the air flow in variable wind speed while the number of parallel fans remain fixed.

E. Tower and Foundation

The calculation of tower mass and the tower cost for a 6 MW generator is shown in [9]. For the 8 MW and 10 MW generators, tower mass and cost are calculated by using the data from Table I and Table III.

The foundation type is assumed a monopile in this study. For a water depth of 30m, the monopile mass, m_{mp} (kg) can be calculated for different turbine ratings, T_{r} and hub height, h_{hub} (given in Table I) as [27],

$$m_{\text{mp}} = \frac{\left((1000T_{\text{r}})^{1.5} + \frac{h_{\text{hub}}^{3.7}}{10} + 2100{d_{\text{w}}}^{2.25} + (1000m_{\text{top}})^{1.13}\right)}{10} \tag{9}$$

where d_{w} is the water depth and m_{top} is the top head mass of the turbine. The substructure and foundation mass, m_{sf} can be found as,

$$m_{\text{sf}} = m_{\text{mp}} + m_{\text{tpos}} \tag{10}$$

where m_{tpos} is the monopole transition piece. The monopile cost and the monopile transition piece cost can be calculated by taking the steel cost from Table III (it is assumed that, the pile is 60% and the transition piece and outfitting steel is 40%).

F. Optimization

It is essential to perform optimization with specific objective function in order to achieve the best performance machine. The optimization process uses an algorithm which takes some initial input to vary within their boundary limit to calculate dependent variables (with consideration of given constraints) to optimize for a specific objective function. The algorithm used in this study is a hybrid algorithm incorporating GA developed by [28] and PS which is

developed in MATLAB. The independent variables and the objective functions for the optimization are described in following section 1 and 2. The flow chart of the optimization procedure is given in Fig. 6. A detailed optimization procedure can be found in [9].

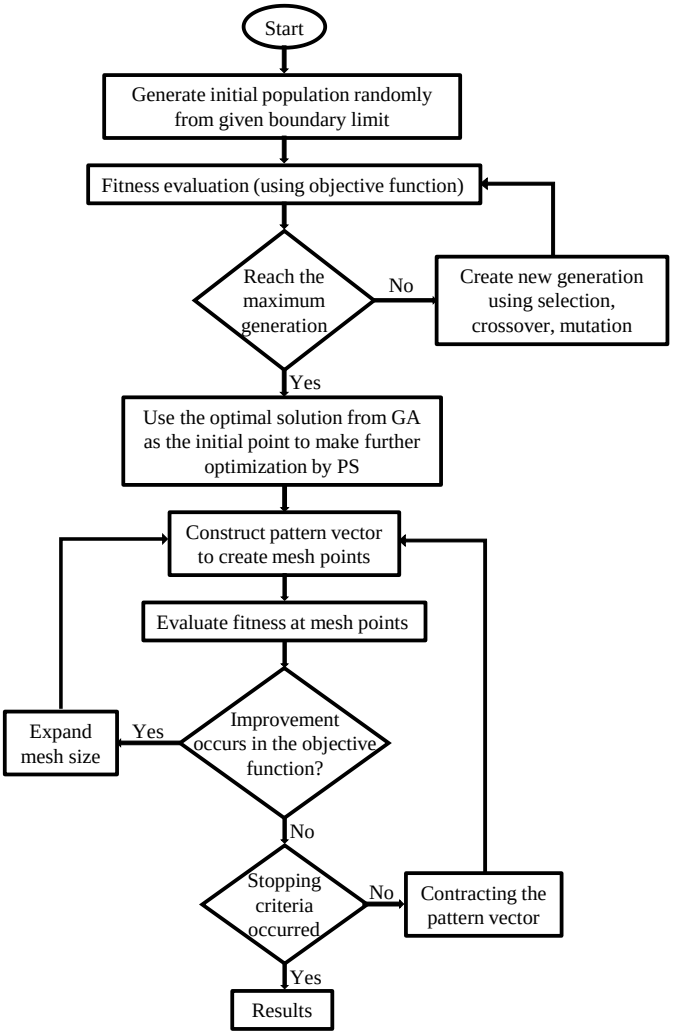

Fig. 6. Flow chart for optimization process

1) Independent Variables and Constraints

Table VII gives the boundary limit of Six independent variables that are used in this study for different power ratings. Where LB stands for the lower boundaries and UB stands for the upper boundaries.

TABLE VII
INDEPENDENT VARIABLES AND LIMITS FOR DIFFERENT POWER RATINGS

Surface mounted Nd-Fe-B generator						
	6 MW		8 MW		10 MW	
Independent variables	LB	UB	LB	UB	LB	UB
Air-gap diameter, D (m)	6	15	6	16	6	17
Axial length, l_s (m)	0.7	1.8	0.7	2	0.7	2.2
Magnet width/pole pitch, w_m/τ_p	0.5	0.9	0.5	0.9	0.5	0.9
Magnet height, h_m (m)	0.01	0.06	0.01	0.08	0.01	0.1
Pole pairs, p (-)	60	100	60	100	60	100
Height of tooth, h_t (m)	0.04	0.09	0.04	0.1	0.04	0.11

To simplify the optimization process, it is assumed that, the air gap clearance is the fixed ratio of the generator diameter. Also using maximum stator and rotor yoke flux densities to avoid saturation condition, which is 1.5 T. The power ratings are made constraints for different rated machine in the optimization run.

2) Objective Functions

McDonald and Bhuiyan [9] compared some objective functions to find the best possible way of machine optimization. Out of four objective functions, this study has chosen two, as these objective functions has produced efficient machine design in terms of cost of energy, losses, active and structural masses, efficiency and annual energy production. The first objective function, F_1 looks for maximum revenue while minimum active material cost over a number of years, P_y for the offshore wind turbine. This is performed for a 15 years' period of time which is multiplied by the revenue of 1 kWh electrical energy, C_E and the annual energy production, E_y,

$$F_1 = C_{PM} + C_{Cu} + C_{Fe} - P_y C_E E_y \quad (11)$$

The 2nd objective function search for the lowest cost of energy, *COE* (the cost incurred to produce per unit energy), which is the ultimate aim of the wind turbine manufacturer,

$$F_2 = COE = \frac{(FCR \times ICC) + AOM}{E_y} \quad (12)$$

where *FCR* represents the fixed charge rate given in Table I, *ICC* is the initial capital cost of the turbine and *AOM* is the annual operation and maintenance cost given in Table I (assumed to be fixed for different machine design). The initial capital cost can be calculated as,

$$ICC = C_{gact} + C_{gstr} + C_{tower} + C_{sf} + C_{fan} + C_{hex} + C_{rt} \quad (13)$$

where C_{gact} is the generator active materials cost, C_{gstr} is the generator structural materials cost, C_{tower} is the tower cost, C_{sf} is the substructure and foundation cost, C_{hex} is the cost of heat exchanger and C_{rt} is the rest of the turbine cost given in Table I.

G. Runs/Investigations

For a SM Nd-Fe-B generator, the optimization run typically takes 7 min in MATLAB 2014 on a 64-bit Windows 7 operating system on a PC with an Intel core i7 3.4GHz processor.

In this study GA gives results near to global optimum solution after 4 generations, the population size is 100, the maximum stall generation is 10 and the function tolerance is 1×10-3. The mutation function is adaptive feasible. For the Pattern Search algorithm, the mesh size expansion factor is 2 and the mesh size contraction factor is 0.5 [29].

In the beginning the optimization program was run for SM Nd-Fe-B generator with rated powers of 6, 8 and 10 MW for both objective functions. After this, the Nd-Fe-B magnet was varied from N35 to N52 (regular magnets) and N35H to N52H ("H" grade magnets) for a 6 MW SM Nd-Fe-B generator (baseline magnet grade in this study is N40H) using the 2nd objective function.

The thermal model is included in the optimization program (using F_2) to calculate required cooling air flow to cool down the magnet's temperature of generator from 120°C to 80°C. The effect on resistance and B_r is also included to calculate the cost of energy of the turbine with cooling. The optimization

program runs in a way, that calculate the required cooling air flow, fan and heat exchanger first to cool down the magnet temperature from120ºC to 80ºC, then change the magnet remanence and resistivity of copper for 80ºC to obtain the overall solution.

III. Results

A. Different Turbine Power Ratings

Table VIII presents the independent variables chosen during the optimization for the both objective functions with different power ratings.

Fig. 7 gives the results after optimization for F_1 and F_2 with different power ratings. F_1 gives negative result, as the revenue is much higher than active material cost. At rated wind speed, the objective function F_1 gives the highest efficiency for all the power ratings. Fig. 8 gives the losses and efficiency curve of a 6 MW Nd-Fe-B generator using F_1 and F_2 and magnet grade N40H. Other generators also follow the similar pattern of efficiency and ratio between copper losses and Iron losses after optimization.

TABLE VIII
INDEPENDENT VARIABLES VS OBJECTIVE FUNCTIONS

Surface mounted Nd-Fe-B generator						
	6 MW		8 MW		10 MW	
Independent variables	F_1	F_2	F_1	F_2	F_1	F_2
Air-gap diameter, D (m)	11.87	10.44	13.22	10.43	11.55	11.74
Axial length, l_s (m)	1.38	1.24	1.63	1.18	1.84	1.55
Magnet width/pole pitch, w_m/τ_p	0.78	0.79	0.8	0.67	0.86	0.77
Magnet height, h_m (m)	0.02	0.018	0.02	0.04	0.038	0.025
Pole pairs, p (-)	82	100	86	88	64	95
Height of tooth, h_t (m)	0.089	0.08	0.1	0.09	0.11	0.1

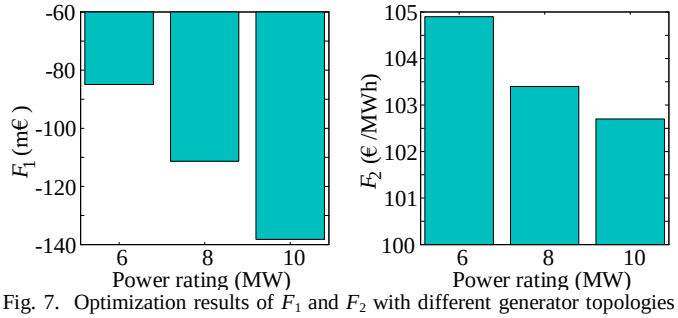

Fig. 7. Optimization results of F_1 and F_2 with different generator topologies and power ratings

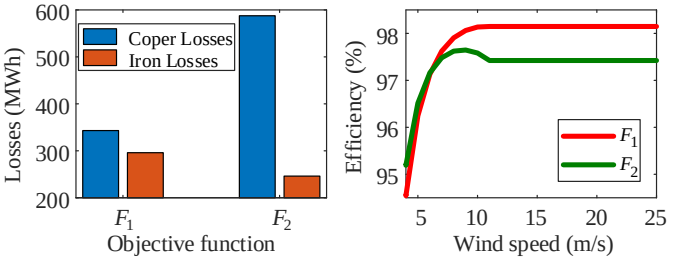

Fig. 8. Losses and efficiency curve of a 6 MW Nd-Fe-B generator after optimization using F_1 and F_2 and magnet grade N40H

Table IX shows the difference of cost and energy production per MW for a SM Nd-Fe-B generator, upgrading from 6 MW to 8 MW and 10 MW (using F_2).

TABLE IX
UPGRADING FROM 6 MW TO 8 MW AND 10 MW: COST AND ENERGY

	8 MW	10 MW
Active materials cost	8.6% increased	12.2% increased
Structural material cost	24.2% increased	26.6% increased
Tower cost	2.2% decreased	3.2% decreased
Substructure and foundation cost	2.1% increased	9.5% increased
Wind firm rest of the turbine capital cost	5.4% decreased	8.2% decreased
Annual energy production	1.8% decreased	2.2% decreased

B. Effect of Different Magnet Grades

Fig. 9 shows the effect of different magnet grades on the cost of energy for a 6 MW SM Nd-Fe-B generator. The results are shown for "H" grade magnet at 120˚C as well as regular and "H" grade magnet at 80˚C (cooled down from 120˚C).

By varying the magnet grade from N35 to N52, the cost of energy using "H" grade magnet decreases up until N48 and then increases for N50 and N52; the cost of energy using regular magnets (at 80˚C) decreases from N35 to N50 and then slightly increases for N52.

Fig. 10 shows the effect of different magnet grades on the magnet mass for a 6 MW SM Nd-Fe-B generator. By varying the magnet grade from N35 to N52, the magnet mass using "H" grade magnet at 120ºC varies from 5 tonnes to 3.4 tonnes. Others also follow the same decreasing trends.

It is found that for a 6 MW SM Nd-Fe-B generator using N40H magnet, a +5% tolerance in magnet's remanence, B_r decrease the turbine cost of energy by 0.03% and a -5% tolerance increase the turbine cost of energy by 0.05%. Also +2 MGOe tolerance in maximum energy product reduce the cost of energy by 0.006% and -2 MGOe tolerance increase the cost of energy by 0.003%.

C. Effect of Temperature and Cooling Cost

Fig. 11 shows the effect of temperature for a 6 MW Nd-Fe-B generator using N40H magnet: (a) shows the power losses at 80°C and 120°C temperatures, (b) shows the required volumetric cooling airflow to cool down the magnet temperature of the generator from 120˚C to 80˚C. It can be seen that the power losses below rated wind speed are variable and hence the required volumetric cooling airflow also varies, (c) shows the trend line of the required cooling air flow for different magnet temperature (d) shows the number of series fan required (5 series fan, where each of the fan curves denotes the number of series fan) the generator to achieve the required volumetric cooling airflow (1.38 m^3/s in this case) to cool down the temperature from 120˚C to 80˚C while the number of parallel fans are fixed (4 parallel fan). It can be seen that the maximum air flow at rated power can be achieved by using maximum number of series fan and this is reduced by subsequently turning off some of the series fans.

In order to reduce the magnet temperature from 120˚C to 80˚C for a 6 MW SM Nd-Fe-B generator using N40 magnet, the required cooling airflow at rated speed is 1.38 m^3/s, the number of parallel fan is 4, the number of series fan is 5 and the number of heat exchanger is 5.

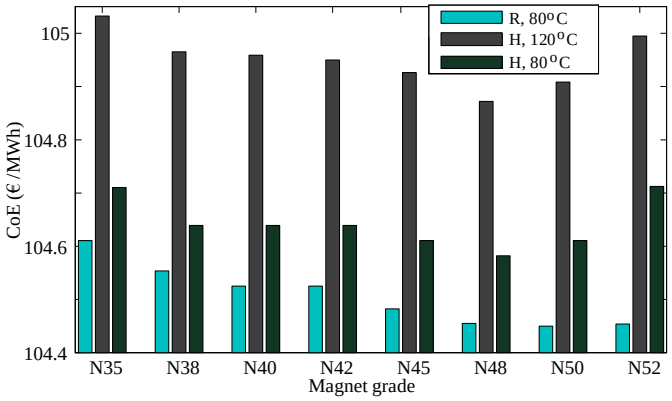

Fig. 9. Effect of different magnet grade on cost of energy

The cost of energy for a 6 MW SM Nd-Fe-B generator including cooling system is given in Fig. 9, and this shows that the cost of energy using "H" grade magnet at 80˚C (using cooling system) is less than the cost of energy at 120˚C without cooling system. The regular magnet at 80˚C (using cooling system) gives the better cost of energy compared to the "H" grade magnet.

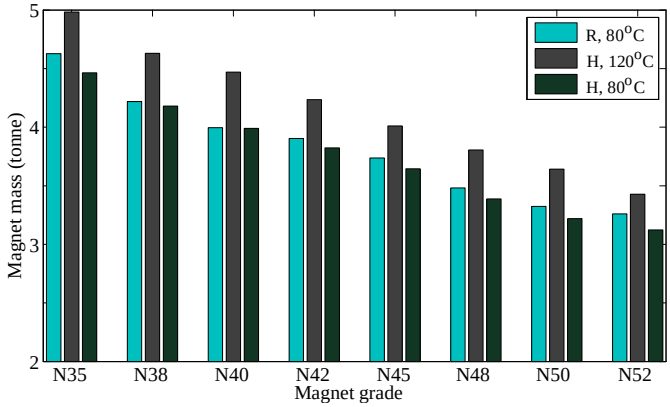

Fig. 10. Effect of different magnet grade on magnet mass

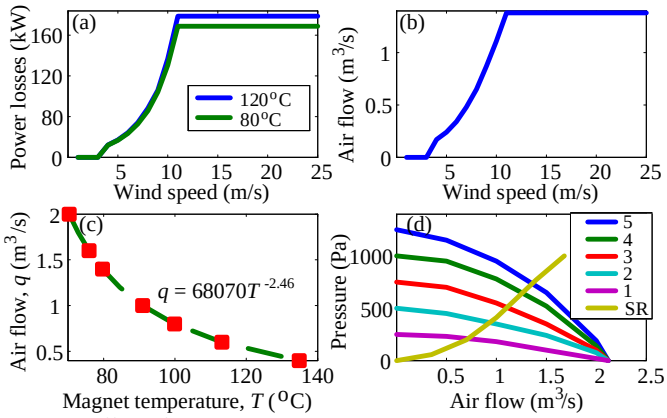

Fig. 11. Effect of Temperature and cooling (a) Power losses at 80°C and 120°C (b) Required volumetric cooling airflow to cool down the magnet temperature from 120˚C to 80˚C (c) Trend line of cooling air flow required for different magnet temperature (d) Fan curves for series fan intersects total system resistance curve (SR) where intersecting point is the volumetric cooling airflow achieved (4 parallel fan and 5 series fan)

IV. Discussions

A. On the Choice of Turbine Power Ratings

The cost of energy marginally decreases when moving from 6 to 8 to 10 MW rated power. Although the per MW cost of the generator's active and structural materials, substructure and foundation cost are increasing with turbine size, this is mitigated by the rest of the turbine cost. The 6 MW turbine gives slightly better revenue per MW over the first 15 years of life than the turbines with higher rated power turbine, but the difference is small.

B. On the Effect of Magnet Grade

The cost of energy of the turbine and the magnet mass slightly decreases by using magnet grades with higher maximum energy product, BH_{max}. Although the magnet price increases for the higher magnet grade, the higher BH_{max} produces higher air-gap flux density and ultimately improves the energy conversion efficiency with lower magnet mass. However, when selecting an Nd-Fe-B grade, the designer should keep in mind that the higher-grade magnets can be more brittle.

C. On the Effect of Temperature and Including Cooling System

The generators that use regular temperature grade Nd-Fe-B magnets generally give lower cost of energy but with slightly higher magnet mass than using "H" grade Nd-Fe-B magnets. The main downside of the regular magnet is the maximum operating temperature which is 80˚C whereas for the "H" grade magnet it is 120˚C. When selecting the working temperature, one needs to make sure that the maximum operating temperature of the magnet is not exceeded, otherwise the magnet can be irreversibly demagnetized. If the rated power and losses of a machine leads to a magnet temperature of 120˚C, then an additional cooling system (or additional levels of cooling) can be implemented to bring it down to 80˚C, allowing the regular temperature grade magnets to be used. This additional cooling system cost and energy consumption accounts for about 0.3% of cost of energy.

In variable wind speeds at below rated power, the generator losses also vary. The required cooling air flow is variable – this can be controlled by varying the number of series fan while number of parallel fans are fixed. The cooling regime can be optimized for minimizing the cost of energy.

As well as facilitating the use of the cheaper, regular temperature grade of magnets, the additional cooling gives two benefits regardless of the temperature grade used in the generators. The cooling helps to reduce the stator winding temperatures, the resistance and hence the copper losses. The lower magnet temperatures also increase the effective remanent flux density due to the negative temperature coefficient of remanence.

When comparing the magnet temperature grades, the regular magnets provide lowest cost of energy. Using the high temperature magnets near to their maximum working temperature (120˚C) leads to higher copper losses and a reduction in remanent flux density. This can be reduced by cooling these machines down to 80˚C. The difference between regular and high temperature magnets at 80˚C is small, and the

use of high temperature magnets may be safer as the magnets will not demagnetize if the cooling system fails.

V. Conclusions

In this paper a methodology for modeling and comparing the design of generators with different power ratings and magnet choice was developed. This involved modeling the specific magnet cost as a function of $BH_{\max}$ and temperature grade; a detailed thermal and cooling system model; integrated into an existing generator and turbine optimization framework.

Based on current price characteristics, the choice of $BH_{\max}$ at or above 48MGOe is optimal. Generally speaking, the generator cost reduces as $BH_{\max}$ increases, while the efficiency of the optimal designs at each value of $BH_{\max}$ is fairly similar. The higher magnet grade produces higher air-gap flux density with lower magnet mass. However, the downside is that the higher-grade magnets can be more brittle.

Based on current price differentials, the regular magnet in a machine cooled down to 80˚C gives the lowest cost of energy. Partly this explained by the lower specific magnet cost of these magnets and partly this is explained by the reduced copper losses and additional remanent flux density when the machine is cooled to 80˚C. The difference in the cost of energy of the regular and high temperature magnets is relatively small, and the high temperature magnets can withstand the elevated temperatures in fault scenarios.

These conclusions are applicable regardless of the power rating of the wind turbine. The larger turbines tend to have lower cost of energy for reasons outside the generator; the costs of the generator itself increases with the power rating.

It is shown that, for a 6 MW SM Nd-Fe-B generator, using higher grade magnet (N35H to N48H) reduce the turbine cost of energy by 0.15% and magnet mass by 32%. It is also found that, using a regular magnet at 80˚C (with cooling) instead of "H" grade magnet at 80˚C can reduce the turbine cost of energy about 0.1%.

VI. References

[1] A. S. McDonald, M.A. Mueller and H. Polinder, "Structural mass in direct-drive permanent magnet electrical generators," *IET Renew. Power Generation,* vol. 2, no. 1, pp. 3-15, Mar. 2008.

[2] R. S. Semken, M. Polikarpova, P. Roytta, J. Alexandrova, J. Pyrhonen, J. Nerg, A. Mikkola and J. Backman, "Direct-drive permanent magnet generators for high-power wind turbines: benefits and limiting factors," *IET Renew. Power Generation,* vol. 6, no. 1, pp. 1-8, Jan. 2012.

[3] M. A. Mueller, A. S. McDonald, D. E. Macpherson, "Structural analysis of low-speed axial-flux permanent-magnet machines," *IEE Proc. – Electr. Power Appl.,* vol. 152, no. 6, pp. 1417–1426, Nov. 2005.

[4] M. Polikarpova, P. Ponomarev, P. Lindh, I. Petrov, W. Jara, V. Naumanen, J. A. Tapia and J. Pyrhonen, "Hybrid Cooling Method of Axial-Flux Permanent-Magnet Machines for Vehicle Applications," *IEEE Trans. Ind. Electron*., vol. 62, no. 12, pp. 7382–7390, Dec. 2015.

[5] A. Grauers, "Design of direct-driven permanent-magnet generators for wind turbines," Ph.D. dissertation, Chalmers Univ. Technol., Goteborg, Sweden, 1996.

[6] Y. Alexandrova, R. S. Semken, and J. Pyrhonen, "Permanent magnet synchronous generator design solution for large direct-drive wind turbines: Thermal behavior of the LC DD-PMSG," *Appl. Therm. Eng*., vol. 65, nos. 1–2, pp. 554–563, 2014.

[7] A. Boglietti, A. Cavagnino, M. Pastorelli, D. Staton, and A. Vagati, "Thermal analysis of induction and synchronous reluctance motors," *IEEE Trans. Ind. Appl*., vol. 42, no. 3, pp. 675–680, May/Jun. 2006.

[8] C. Kral, A. Haumer and T. Bauml, "Thermal Model and Behavior of a Totally-Enclosed-Water-Cooled Squirrel-Cage Induction Machine for Traction Applications, *IEEE Trans. Ind. Electron*.", vol. 55, no. 10, pp. 3555-3565, Oct. 2008.

[9] A. McDonald and N. A. Bhuiyan, "On the Optimization of Generators for Offshore Direct Drive Wind Turbines," *IEEE Trans. Energy Convers., vol*. 32, no. 1, pp. 348-358, Mar. 2017.

[10] H. Polinder, "Principles of electrical design of permanent magnet generators for direct drive renewable energy systems," in *Electrical Drives for Direct Drive Renewable Energy Systems*, M. Mueller, H. Polinder, Ed. UK: Woodhead Publishing, 2013, ch. 2, pp. 43.

[11] H. Polinder, F. F. A. Van der Pijl, G. J. De Vilder, and P.J. Tavner, "Comparison of direct-drive and geared generator concepts for wind turbines," *IEEE Trans. Energy Convers.*, vol. 21, no. 3, pp. 725-733, Sept. 2006.

[12] H. Li, Z. Chen, and H. Polinder, "Optimization of multibrid permanent-magnet wind generator systems," *IEEE Trans. Energy Convers.*, vol. 24, no. 1, pp. 82–92, Mar. 2009.

[13] A. Zavvos, A. McDonald, and M. Mueller, "Optimisation tools for large permanent magnet generators for direct drive wind turbines," *IET Renew. Power Generation*, vol. 7, no. 2, pp. 163-171, Mar. 2013.

[14] J. Carroll, A. McDonald, D. McMillan, T. Stehly, C. Mone, and B. Maples, *"*Cost of energy for offshore wind turbines with different drive train types*,"* presented at Eur. Wind Energy Assoc. Annu. Conf., Paris, France, Nov. 17-20, 2015.

[15] L. Fingersh, M. Hand, A. Laxson, "Wind turbine design cost and scaling model," Nat. Renew. Energy Lab., Golden, CO, USA, Tech. Rep. NREL/TP-500-40566, Dec. 2006.

[16] *Finite Element Method Magnetics* v4.2. (2016) [Online] Available at: http://www.femm.info/wiki/HomePage

[17] N. A. Bhuiyan and A. McDonald, "Assessment of the Suitability of Ferrite Magnet Excited Synchronous Generators for Offshore Wind Turbines," presented at Eur. Wind Energy Assoc. Offshore Conf., Copenhagen, Denmark, Mar. 10-12, 2015.

[18] Arnold Magnetic Technologies, Rochester, NY, USA. Neodymium Iron Boron Magnets. (2016) [Online]. Available at: http://www.arnoldmagnetics.com/en-us/Products/Neodymium-Magnets, Accessed on: Oct. 10, 2016.

[19] O. Gutfleisch, "Controlling the properties of high energy density permanent magnetic materials by different processing routes," *J. Phys. D, Appl. Phys.*, vol. 33, p. R157, 2000.

[20] J. J. Becker, "Rare-Earth-Compound Permanent Magnets," *J. Appl. Phys.*, vol. 41, no. 3, pp. 1055-1064, 1970.

[21] Magnet Expert Ltd, Tuxford, Nottinghamshire, UK. *Neodymium Magnets*. (2016) [Online]. Available at: https://www.magnetexpert.com/technical-advice-i685/materials- information-i682, Accessed on: Nov. 15, 2016.

[22] Ningbo ZhaoBao Magnet Co., Ltd, Ningbo, Zhenhai, China. *Neodymium Magnets*. (2016) [Online]. Available at: http://www.zhaobao-magnet.com/, Accessed on: Nov. 15, 2016.

[23] D. Staton and A. Cavagnino, "Convection heat transfer and flow calculations suitable for electric machines thermal models," *IEEE Trans. Ind. Electron.*, vol. 55, no. 10, pp. 3509–3516, Oct. 2008.

[24] *Woods Practical Guide to Fan Engineering*, Woods Colchester Ltd., Colchester, U.K., Jun. 1960.

[25] Torin-Sifan, Swindon, Wiltshire, UK. *Fan deck DPN160-222 EC*. (2016) [Online]. Available at: http://www.torin-sifan.com/display.asp?product=78 , Accessed on: Oct. 25, 2016.

[26] Vent-Axia, Crawley, Sussex, UK. *HR500EP/IP Passive HR Unit*. (2016) [Online]. Available at: https://www.vent-axia.com/sites/default/files/mvhr_-_hr500ep_ip.pdf , Accessed on: Oct. 30, 2016.

[27] M. Maness, B. Maples, and A. Smith, "NREL Offshore Balance-of-System Model," Nat. Renew. Energy Lab., Golden, CO, USA, Tech. Rep. NREL/TP-6A20-66874, Jan. 2017.

[28] A. Chipperfield, P. Fleming, H. Pohlheim, C. Fonseca, *Genetic Algorithm Toolbox for use with MATLAB.* (1994) [Online]. Available at: http://codem.group.shef.ac.uk/index.php/ga-toolbox

[29] MathWorks, Natick, MA, USA. Global Optimization Toolbox User's guide. (2016) [Online]. Available at: http://in.mathworks.com /help/pdf_doc/gads/gads_tb.pdf, Accessed on: Mar. 28, 2016.

Nurul Azim Bhuiyan received the B.Sc. degree in Electrical and Electronic Engineering from the Ahsanullah University of Science and Technology, Dhaka, Bangladesh in 2007, M.Sc. degree in Sustainable Electrical Power from the Brunel University, London, U.K. in 2011 and Ph.D. degree in modelling, design and optimization of generators for large offshore wind turbine from the University of Strathclyde, Glasgow, U.K in 2018. He is currently working at Swansea University, Swansea, U.K.

Alasdair McDonald received the M.Eng. degree in Electrical and Mechanical Engineering from the University of Durham, U.K., in 2004, and a Ph.D. degree in design and modeling of direct drive generators from the University of Edinburgh, UK., in 2008. He is a Senior lecturer in the Wind and Marine Energy Systems Doctoral Training Centre, University of Strathclyde, Glasgow, U.K.